Electron-impact excitation of beryllium and its ions

C. P. Ballance and D. C. Griffin
Department of Physics, Rollins College, Winter Park, Florida 32789, USA

J. Colgan, S. D. Loch, and M. S. Pindzola
Department of Physics, Auburn University, Auburn, Alabama 36849, USA
(Received 24 August 2003; published 18 December 2003)

Inelastic electron scattering from light atomic species is of fundamental importance and has significant applications in fusion-plasma modeling. Therefore, it is of interest to apply advanced nonperturbative, close-coupling methods to the determination of electron-impact excitation for these atoms. Here we present the results of *R* matrix with pseudostate (RMPS) calculations of electron-impact excitation cross sections through the $n=4$ terms in Be, Be^{+}, Be^{2+}, and Be^{3+}. In order to determine the effects of coupling of the bound states to the target continuum in these species, we compare the RMPS results with those from standard *R*-matrix calculations. In addition, we have performed time-dependent close-coupling calculations for excitation from the ground and the metastable terms of Be^{+} and the metastable term of Be^{3+}. In general, these results are found to agree with those from our RMPS calculations. The full set of data resulting from this work is now available on the Oak Ridge National Laboratory Controlled Fusion Atomic Data Center web site, and will be employed for collisional-radiative modeling of Be in magnetically confined plasmas.

DOI: 10.1103/PhysRevA.68.062705 PACS number(s): 34.80.Kw

I. INTRODUCTION

Beryllium has been used as a surface material at JET and is being proposed for the plasma-facing walls for ITER. For that reason, experiments on beryllium are being conducted at the PISCES-B plasma-surface interaction research facility at the University of California at San Diego. Collisional-radiative modeling of beryllium is an important part of that effort, and this requires accurate electron-impact excitation, ionization, and recombination data. Recently, we completed a series of time-dependent close-coupling (TDCC) and *R* matrix with pseudostate (RMPS) calculations of the ionization of beryllium and all its ions [1]. In addition, dielectronic recombination data for beryllium have been generated in the distorted-wave approximation [2], using the program AUTOSTRUCTURE [3]. In this paper, we report on the results of electron-impact excitation calculations using the RMPS method for Be, Be^{+}, Be^{2+}, and Be^{3+}, and the TDCC method for Li-like and H-like beryllium.

Because of its toxic nature, very few experiments of electron collisions with beryllium have been completed. The only experimental excitation data of which we are aware are those of Taylor *et al.* [4] for the $2s \rightarrow 2p$ transition in Be^{+}. However, there has been a number of theoretical studies of electron-impact excitation for both Be and Be^{+}. For the neutral species, this includes the *R*-matrix calculations of Fon *et al.* [5], the distorted-wave (DW) calculations by Clark and Abdallah [6], the RMPS calculations by Bartschat *et al.* [7,8], and the convergent close-coupling (CCC) calculations by Fursa and Bray [9,10]. In addition, CCC data for a large number of transitions from the ground and $2s2p$ configurations of Be are available on the web page of Bray [11]. For Be^{+}, there have been the close-coupling calculations by Mitroy and Norcross [12], the *R*-matrix calculations reported in a paper by Berrington and Clark [13], the DW calculations by Clark and Abdallah [6], and the RMPS and CCC calculations by Bartschat and Bray [14]. To our knowledge, there have been no prior close-coupling calculations for excitation of He-like Be^{2+}. However, there have been the DW calculations of Pradhan *et al.* [15] and Badnell [16]. For Be^{3+}, there have been the *R*-matrix and DW calculations presented in the paper by Berrington and Clark [13]. More recently, RMPS calculations for Be^{3+} were reported as part of a study of the hydrogen isoelectronic sequence [17].

The purpose of the present investigation is twofold. On the fundamental side, we wish to study the effects of coupling of the bound states to the high-Rydberg states and the target continuum, for similar transitions along the Be isonuclear sequence. For that reason, we have compared the results of our RMPS calculations with those from a standard *R*-matrix calculation that employed the same configuration-interaction description of the target, but did not include pseudostates in the close-coupling expansion to represent the high-Rydberg states and the target continuum. Furthermore, as an independent check of our RMPS results in the intermediate-energy range, we have performed TDCC calculations from the ground and metastable terms for Be^{+} and from the metastable term of Be^{3+}.

On the applied side, we wish to generate excitation data that can be used for the modeling of Be and its ions in magnetically confined fusion plasmas. The TDCC, CCC, and RMPS methods are all capable of producing cross sections that include the effects of coupling the target continuum, which are important for neutral atoms and low-charge-state ions at intermediate energies. However, of these three, only the RMPS method provides an efficient method for including an accurate description of the resonance contributions, which can dominate the low-energy cross sections, especially for nondipole transitions in ionic species. Nevertheless, the application of electron-impact excitation data to plasma modeling places special demands on RMPS scattering calculations. For accuracy at low temperatures, the outer-region

portion of the calculation must be carried out over a sufficiently fine energy mesh to resolve the majority of narrow resonances. For accuracy at higher temperatures, one must incorporate a large pseudostate expansion of the target continuum and a large basis-set representation of the $(N+1)$-electron continuum. Furthermore, one must include contributions from high partial waves. These requirements can lead to very large RMPS calculations, even for relatively simple target species, providing a real challenge for current massively parallel computing platforms.

The remainder of this paper is organized as follows. In the following section, we give a brief description of our RMPS, *R*-matrix, and TDCC calculations. In Sec. III, we present the results of our calculations and compare them with each other and with the results of CCC calculations, where available. In Sec. IV, we summarize our findings and discuss their implications.

II. DESCRIPTION OF THE CALCULATIONS

A. Target states for the RMPS and *R*-matrix calculations

All the target states employed in our RMPS and *R*-matrix calculations were generated using the program AUTOSTRUCTURE [3]. For Be and all its ions, we employed spectroscopic radial wave functions for all configurations involving $1s$ through $4f$ orbitals. For Be^{2+}, in addition to the $1snl$ configurations, we also included the $2s^2$ and $3s^2$ configurations in order to improve the target structure. For Be and Be^{2+}, the spectroscopic radial wave functions were determined from local potentials using Slater-type orbitals; for Be^{+}, they were calculated using a Thomas-Fermi-Dirac-Amaldi statistical potential; and for Be^{3+}, they were, of course, numerical hydrogenic radial wave functions with $Z=4$.

For the pseudo-orbitals, we first generated a set of nonorthogonal Laguerre radial wave functions of the form

$$P_{nl}(r)=N_{nl}(\lambda_l Zr)^{l+1}e^{-\lambda_l Zr/2}L_{n+l}^{2l+1}(\lambda_l Zr). \qquad (1)$$

In this equation, $Z=z+1$, where z is the residual charge on the ion, $L_{n+l}^{2l+1}(\lambda_l Zr)$ represents the Laguerre polynomial, and N_l is a normalization constant. These Laguerre orbitals were then orthogonalized to the spectroscopic orbitals and to each other. The screening parameters λ_l were adjusted so that the $n=5$ and $n=6$ pseudostates (in the case of Be, the $2snl$ configurations only) were bound. This procedure leads to a set of $n=5$ terms that are nearly spectroscopic and a set of $n=6$ terms that are used to approximate the effects of coupling to the higher-Rydberg states.

In the case of neutral beryllium, we included pseudostates for all $2snl$ configurations from $n=5$ through $n=11$ and all $2pnl$ configurations from $n=5$ through $n=10$, with $l=0$ to $l=4$; this leads to a total of 280 spectroscopic and pseudoterms, 241 of which are above the ionization limit. For Be^{+}, we included pseudostates for all nl configurations from $n=5$ to $n=12$ and $l=0$ to $l=4$, for a total of 49 terms, 30 of which are in the continuum. For Be^{2+}, we included pseudostates for the $1s5l$ configurations for $l=0$ to $l=4$ and all $1snl$ configurations from $n=6$ to $n=11$, and $l=0$ to $l=5$; this leads to a total of 103 spectroscopic and pseudoterms, 60 of which are above the ionization limit. For Be^{3+}, we included pseudostates for the $5l$ configurations from $l=0$ to $l=4$ and all nl configurations from $n=6$ to $n=12$, and $l=0$ to $l=5$; this yields a total of 57 spectroscopic and pseudoterms, 36 of which are in the continuum.

Originally, for the He-like and H-like ions, we had hoped to calculate excitation to the $n=5$ configurations, which are represented fairly accurately by pseudostates. For these configurations, coupling to the higher $l=5$ pseudostates could have some effect and were, therefore, included in our pseudostate expansions for these ions. However, the excitation cross sections to a number of the $n=5$ terms were found to have large pseudoresonances and were too unreliable to be included in our final results. Coupling to the $l=5$ pseudostates should have negligible effects on the results reported here.

B. RMPS and *R*-matrix scattering calculations

All *R*-matrix scattering calculations reported here were performed with our parallel versions of the RMATRX I suite of programs [18]. The RMPS calculation for Be included 280 terms in the close-coupling (CC) expansion. In addition, we performed an *R*-matrix calculation that included all 280 terms in the configuration-interaction (CI) expansion of the target, but only the 29 terms through the $2s5l$ configurations in the close-coupling expansion. By comparing the results of these two calculations, we can determine the effect of coupling to the high-Rydberg states ($n>5$) and the target continuum on excitation between the lowest 19 terms (through the $2s4l$ configurations). In order to remove the pseudoresonances in the 29-term *R*-matrix calculation that are attached to the 251 terms included in the CI expansion, but not in the 29-term CC expansion, we employed the pseudoresonance removal method described by Gorczyca *et al.* [19].

For the inner-region portion of these calculations, the size of the *R*-matrix box was 71.7 a.u., and 45 basis orbitals were used to represent the $(N+1)$-electron continuum for each value of the angular momentum. Calculations with full exchange were performed for all $LS\Pi$ partial waves up to $L=11$. In order to improve on the accuracy of the calculations, the term energies were adjusted to the experimental values. In the outer region, we employed 1280 energy mesh points in the energy range between the first excited term and the highest-energy term arising from the $2s5l$ configurations, for a mesh spacing of 3.5×10^{-4} Ry. Above this energy, we employed 192 mesh points up to a maximum energy of 2.5 Ry, with a mesh spacing of 9.7×10^{-3} Ry. The long-range multipole potentials were included perturbatively in the outer-region solutions for all partial waves.

A partial-wave expansion up to $L=11$ is not sufficiently complete to allow for the determination of cross sections up to the highest-energy run for Be of 2.5 Ry. Thus, for the 29-term *R*-matrix calculation, we performed a calculation without exchange for all partial waves from $L=12$ to $L=50$; this was then topped up as follows: the dipole-allowed transitions were topped up using a method originally described by Burgess [20]; the nondipole transitions were topped up assuming a geometric series in L, using energy

ratios, with a special procedure for handling transitions between nearly degenerate terms based on the degenerate limiting case [21]. In order to include the high partial-wave contributions to the RMPS calculation, we performed a 280-term RMPS calculation without exchange from $L=12$ to $L=20$, followed by a 29-term R-matrix calculation without exchange from $L=21$ to $L=50$ with topup, as described above.

The RMPS and R-matrix calculations performed for the ions of beryllium were similar in nature to the description given above. For Be^+, we included 49 terms in the RMPS CC expansion and 14 terms in the R-matrix CC expansion. In the inner region, the size of the R-matrix box was 41.5 a.u., and again, 45 basis orbitals were used to represent the $(N+1)$-electron continuum. Full exchange calculations were performed up to $L=11$ and nonexchange calculations with topup were performed from $L=12$ to $L=50$. In the outer region, a mesh spacing of 9.0×10^{-4} Ry was used in the lower-energy range and 1.9×10^{-2} Ry at higher energies to a maximum of 6 Ry.

For Be^{2+}, we included 103 terms in the RMPS CC expansion and 29 terms in the the R-matrix CC expansion. In the inner region, the size of the R-matrix box was 25.9 a.u., and 45 basis orbitals were used to represent the $(N+1)$-electron continuum. The range of L values for the exchange and nonexchange parts of the calculations were the same as for Be^+. In the outer region, a mesh spacing of 1.0×10^{-3} Ry was employed in the lower-energy range and 5.0×10^{-2} Ry at higher energies to a maximum of 18.4 Ry.

Finally for Be^{3+}, we included 57 terms in the RMPS CC expansion and 15 terms in the R-matrix CC expansion. In the inner region, the size of the R-matrix box was 21.4 a.u., and 51 basis orbitals were used to represent the $(N+1)$-electron continuum. The range of L values for the exchange and nonexchange portions of the calculations were the same as for Be^+ and Be^{2+}. In the outer region, a mesh spacing of 5.0×10^{-4} Ry was employed in the lower-energy range and 1.4×10^{-2} Ry at higher energies to a maximum of 30 Ry.

C. TDCC scattering calculations

The time-dependent close-coupling method used to determine ionization of ions in the Be isonuclear sequence has been discussed in detail [1]. Our technique to extract excitation cross sections from the time-dependent scattering calculations has also been discussed for the case of neutral lithium [22]. Here we review the important elements of our method.

Both the TDCC calculations for Be^+ and Be^{3+} begin by constructing a complete set of bound and continuum orbitals for each ion. For Be^+, a complete set of orbitals is generated by diagonalizing the Hartree-Fock equation in the presence of a frozen $\underline{Be}^{2+}$ $1s^2$ core. A pseudopotential is used to generate the $\overline{ns}$ orbitals in order to eliminate the inner node of the wave function. This prevents unphysical excitation of filled subshells during time propagation of the close-coupled equations. By a suitable adjustment of a coefficient in the local exchange potential, the ionization threshold from the ground state of Be^+ was tuned to the experimental value. For Be^{3+} a complete set of orbitals is found by simply diagonalizing the one-dimensional hydrogenic Hamiltonian with $Z=4$.

The total two-electron wave function for the valence and continuum electron is expanded in coupled spherical harmonics in the standard manner [22]. The time propagation of the radial part of the wave function, $P^{LS}_{l_1l_2}(r_1,r_2,t)$, is then governed by

$$i\frac{\partial P^{LS}_{l_1l_2}(r_1,r_2,t)}{\partial t}=T_{l_1l_2}(r_1,r_2)P^{LS}_{l_1l_2}(r_1,r_2,t)+\sum_{l_1',l_2'}U^{L}_{l_1l_2,l_1'l_2'}(r_1,r_2)P^{LS}_{l_1'l_2'}(r_1,r_2,t), \tag{2}$$

where $T_{l_1l_2}(r_1,r_2)$ contains all kinetic energy, centrifugal barrier, nuclear, direct Hartree, and local exchange operators, and $U^{L}_{l_1l_2,l_1'l_2'}(r_1,r_2)$ couples the various (l_1l_2) scattering channels. At a suitable time $t=T$ after the collision, which depends on the energy of the incoming electron, the excitation cross section from the state in question can be determined by

$$\sigma_{nl}(L)=\frac{\pi}{4k^2}(2L+1)\sum_S\sum_m(2S+1)\wp^{LS}_{nlm}, \tag{3}$$

where $\wp^{LS}_{nlm}$ is the probability of finding one electron in a bound state and the other in the continuum. This probability is found by projecting the two-electron radial wave functions at $t=T$ directly onto products of bound and continuum states.

For our calculations on Be^+, a uniform mesh of $\Delta r=0.2$ with 512 points was employed. TDCC calculations were made up to and including $L=10$. In our ionization calculations for Be^+, it was found that TDCC calculations were necessary only up to $L=6$, with the contribution from the higher partial waves adequately represented by distorted-wave calculations [1]. For excitation cross sections, however, the convergence by partial wave of the time-dependent results to the distorted-wave results is slower for some of the transitions considered here. Therefore, it was necessary to extend the time-dependent calculations up to $L=10$. The contribution to the cross section for the higher partial waves for most of the transitions is then given by distorted wave. For the $2s\rightarrow nd$ transitions, an extrapolation of the TDCC calculations to the distorted-wave calculations at $L\geqslant15$ was made using a cubic spline fit, following previous work [22]. This was necessary because, for these transitions, the TDCC and distorted-wave partial-wave cross sections are still not completely converged, even at $L=10$.

Our calculations on Be^{3+} were made with a uniform mesh of $\Delta r=0.1$ with 512 points. Even with this relatively fine mesh, it was found that the $1s$ orbital of Be^{3+} was still not well represented, with the energy of this orbital being almost 4% above the experimental value. However the $2s$ orbital of Be^{3+} was much better, with the energy within 1% of experi-

TABLE I. Energies in Rydbergs for the first 19 terms in Be relative to the $2s^2\,{}^1S$ ground term.

No.	Term	Energy (Expt. [29])	Energy (Theor.)	Diff.
1	$2s^2\,{}^1S$	0.0000	0.0000	0.0000
2	$2s2p\,{}^3P$	0.2003	0.1998	−0.0005
3	$2s2p\,{}^1P$	0.3879	0.3992	0.0113
4	$2s3s\,{}^3S$	0.4746	0.4848	0.0102
5	$2s3s\,{}^1S$	0.4983	0.5069	0.0086
6	$2p^2\,{}^1D$	0.5184	0.5208	0.0024
7	$2s3p\,{}^3P$	0.5368	0.5467	0.0099
8	$2p^2\,{}^3P$	0.5440	0.5535	0.0095
9	$2s3p\,{}^1P$	0.5485	0.5583	0.0098
10	$2s3d\,{}^3D$	0.5655	0.5749	0.0094
11	$2s3d\,{}^1D$	0.5871	0.5983	0.0112
12	$2s4s\,{}^3S$	0.5878	0.5986	0.0108
13	$2s4s\,{}^1S$	0.5946	0.6048	0.0102
14	$2s4p\,{}^3P$	0.6088	0.6193	0.0105
15	$2s4p\,{}^1P$	0.6109	0.6211	0.0102
16	$2s4d\,{}^3D$	0.6191	0.6294	0.0103
17	$2s4f\,{}^3F$	0.6219	0.6325	0.0106
18	$2s4f\,{}^1F$	0.6219	0.6325	0.0106
19	$2s4d\,{}^1D$	0.6268	0.6381	0.0113
Ionization energy		0.06852	0.6952	0.0100

ment. In order to represent the $1s$ orbital more accurately, a finer radial mesh must be employed. However this severely reduces the time step that must be used in the time-dependent propagation, which makes the calculations much more computationally demanding. For this reason, we chose only to examine excitation calculations from the $2s$ term of Be^{3+}. Time-dependent calculations were made up to and including $L=8$, with the same procedure employed as before to determine the contribution from the higher partial waves. It should be noted that for both sets of time-dependent calculations described here, the Fourier-transform method, as discussed in Ref. [1], was used to extract the excitation cross sections for several energies from a single time propagation.

III. RESULTS

In Tables I–III, we compare our term energies, calculated using the target states employed in our RMPS calculations, with the experimental values for all terms from the ground term through $n=4$ in Be, Be^+, and Be^{2+}. The theoretical and experimental ionization energies are also given in these tables. The average percentage error between experimental and theoretical term energies is 1.7% for Be, but only 0.2% for Be^+, and 0.1% for Be^{2+}. We note in the case of neutral beryllium that, with the exception of two excited terms, the energies are all high with respect to the ground term by about 0.01 Ry; in addition, the theoretical ionization energy is high by the same amount. As mentioned previously, we have shifted the theoretical threshold energies to the experimental values in the scattering calculations. However, this procedure does not shift the $(N+1)$-electron resonances that are included explicitly in the scattering calculations, and this can lead to errors in the size and position of the resonance contributions. However, this should not have a large effect in the case of Be since the resonance contributions in a neutral species are less pronounced than they are in ions.

TABLE II. Energies in Rydbergs for the first nine terms in Be^+ relative to the $2s$ ground term

No.	Term	Energy (Expt. [29])	Energy (Theor.)	Diff.
1	$2s$	0.0000	0.0000	0.0000
2	$2p$	0.2910	0.2941	0.0031
3	$3s$	0.8040	0.8038	−0.0002
4	$3p$	0.8793	0.8798	0.0005
5	$3d$	0.8935	0.8935	0.0000
6	$4s$	1.0522	1.0519	−0.0003
7	$4p$	1.0822	1.0822	0.0000
8	$4d$	1.0882	1.0880	−0.0002
9	$4f$	1.0885	1.0881	−0.0004
Ionization energy		1.3385	1.3381	−0.0004

In Table IV, we present our absorption oscillator strengths, calculated in the length gauge using our RMPS target states, for a set of transitions in Be for which other calculated results are available. They are compared to those from a large configuration-interaction calculation, using a model potential, by Chen [23] and those from a large multiconfiguration Hartree-Fock (MCHF) calculation that are given on the MCHF collection web site [24] and described in a paper by Tachiev and Froese Fischer [25]. In general, the agreement of our oscillator strengths with those from these two large structure calculations seems quite satisfactory. The

TABLE III. Energies in Rydbergs for the first 19 terms in Be^{2+} relative to the $1s^2\,{}^1S$ ground term.

No.	Term	Energy (Expt. [29])	Energy (Theor.)	Diff.
1	$1s^2\,{}^1S$	0.0000	0.0000	0.0000
2	$1s2s\,{}^3S$	8.7163	8.7013	−0.0150
3	$1s2s\,{}^1S$	8.9412	8.9202	−0.0210
4	$1s2p\,{}^3P$	8.9611	8.9599	−0.0012
5	$1s2p\,{}^1P$	9.0895	9.1185	0.0290
6	$1s3s\,{}^3S$	10.2170	10.2240	0.0070
7	$1s3s\,{}^1S$	10.2764	10.2809	0.0045
8	$1s3p\,{}^3P$	10.2818	10.2910	0.0092
9	$1s3d\,{}^3D$	10.3099	10.3221	0.0122
10	$1s3d\,{}^1D$	10.3106	10.3236	0.0130
11	$1s3p\,{}^1P$	10.3191	10.3353	0.0162
12	$1s4s\,{}^3S$	10.7101	10.7204	0.0103
13	$1s4s\,{}^1S$	10.7348	10.7474	0.0126
14	$1s4p\,{}^3P$	10.7363	10.7474	0.0111
15	$1s4d\,{}^3D$	10.7480	10.7601	0.0121
16	$1s4d\,{}^1D$	10.7484	10.7609	0.0125
17	$1s4f\,{}^1F$	10.7485	10.7607	0.0122
18	$1s4f\,{}^3F$	10.7485	10.7606	0.0121
19	$1s4p\,{}^1P$	10.7514	10.7657	0.0141
Ionization energy		11.3110	11.3232	0.0122

TABLE IV. Absorption oscillator strengths for Be.

Transition	Present	Chen[a]	% Diff.[b]	MCHF[c]	% Diff.[d]
$2s^2\ ^1S$-$2s2p\ ^1P$	1.37	1.38	0.5	1.38	0.9
$2s^2\ ^1S$-$2s3p\ ^1P$	1.12[−2][e]	9.01[−3]	21.7	8.99[−3]	21.9
$2s^2\ ^1S$-$2s4p\ ^1P$	2.00[−4]	2.30[−4]	14.0		
$2s2p\ ^3P$-$2s3s\ ^3S$	7.56[−2]	8.23[−2]	8.5	8.41[−2]	10.6
$2s2p\ ^3P$ -$2s3d\ ^3D$	2.99[−1]	2.95[−1]	1.3	3.00[−1]	0.3
$2s2p\ ^3P$-$2s4s\ ^3S$	1.05[−2]	1.16[−2]	10.0		
$2s2p\ ^3P$-$2s4d\ ^3D$	9.59[−2]	9.55[−2]	0.4		
$2s2p\ ^1P$-$2s3s\ ^1S$	1.20[−1]	1.18[−1]	1.7	1.15[−1]	4.3
$2s2p\ ^1P$-$2s3d\ ^1D$	3.86[−1]	4.10[−1]	6.0	3.96[−1]	2.6
$2s2p\ ^1P$-$2s4s\ ^1S$	7.70[−3]	9.82[−3]	24.2		
$2s2p\ ^1P$-$2s4d\ ^1D$	1.69[−1]	1.74[−1]	2.9		
$2s3s\ ^3S$-$2s3p\ ^3P$	1.02	1.13	9.9	1.14	11.1
$2s3s\ ^3S$-$2s4p\ ^3P$	1.78[−3]	3.01[−3]	51.4		
$2s3s\ ^1S$-$2s3p\ ^1P$	9.08[−1]	9.58[−1]	5.4	9.47[−1]	4.2
$2s3s\ ^1S$-$2s4p\ ^1P$	1.30[−2]	9.88[−3]	27.3		
$2s3p\ ^3P$-$2s3d\ ^3D$	4.83[−1]	5.01[−1]	3.7	5.14[−1]	6.2
$2s3p\ ^3P$-$2s4s\ ^3S$	2.08[−1]	2.15[−1]	3.3		
$2s3p\ ^3P$-$2s4d\ ^3D$	1.42[−1]	1.31[−1]	8.1		
$2s3p\ ^1P$-$2s3d\ ^1D$	6.91[−1]	6.87[−1]	0.6	6.81[−1]	1.5
$2s3p\ ^1P$-$2s4s\ ^1S$	2.04[−1]	2.09[−1]	2.4		
$2s3p\ ^1P$-$2s4d\ ^1D$	9.10[−3]	1.80[−2]	65.7		
$2s3d\ ^3D$-$2s4p\ ^3P$	7.61[−2]	8.15[−2]	6.9		
$2s3d\ ^1D$-$2s4p\ ^1P$	2.17[−1]	1.98[−1]	9.2		
$2s4s\ ^3S$-$2s4p\ ^3P$	1.63	1.61	1.1		
$2s4s\ ^1S$-$2s4p\ ^1P$	1.42	1.43	1.3		
$2s4p\ ^3P$-$2s4d\ ^3D$	8.07[−1]	8.17[−1]	1.2		
$2s4p\ ^1P$-$2s4d\ ^1D$	1.16	1.20	3.5		

[a]From the calculations of Chen [23].
[b]Percentage difference between present values and those of Chen.
[c]See Ref. [24].
[d]Percentage difference between present and MCHF values.
[e]$a[b]$ denotes $a\times10^b$.

average percentage difference between our values and those of Chen is 11%; furthermore, only 6 out of 27 values differ by more than 10%. For the ten transitions provided in the MCHF collection, the average percentage difference is 6%.

Our absorption oscillator strengths for Be^+ and Be^{2+}, also calculated in the length gauge using our RMPS target states, are shown in Tables V and VI, respectively; they are compared to values given on the NIST web site [26]. In general, the present values are in excellent agreement with the NIST data for both ions. The one exception is the $1s2s\ ^1S$-$1s3p\ ^1P$ transition in Be^{2+}, where our value is only 40% of the NIST value. In light of the excellent agreement between the oscillator strengths for the other nine transitions in this ion, we are puzzled by this discrepancy. We made several different structure calculations in order to investigate this problem. For example, we varied the scaling parameters in the Slater-type orbitals used to generate the local potential and found that this oscillator strength was insensitive to these changes. We also calculated this particular oscillator strength using Hartree-Fock spectroscopic orbitals as well as those generated from a Thomas-Fermi-Dirac-Amaldi statistical potential, and found only very small variations from the one reported here. Thus the large difference between the present and NIST value for this particular transition remains unclear. It should also be mentioned that we compared length and velocity oscillator strengths for beryllium and these two beryllium ions and found overall good agreement, including those for the $1s2s\ ^1S$-$1s3p\ ^1P$ transition in Be^{2+}.

The amount of collisional data generated from the present work is far too large to be reported here. However, our RMPS results are now available in the form of Maxwell-averaged effective collision strengths on the Oak Ridge National Laboratory Controlled Fusion Atomic Data Center web site [27]. Here we will focus on comparisons of cross sections determined from the RMPS method with those obtained from the standard *R*-matrix method, and those from the present TDCC and earlier CCC calculations. Out of the many transitions included in these calculations, we have tried to select those that will provide the most complete information regarding the effects of coupling to the target continuum as a function of ionization stage.

In Fig. 1, we present results for the excitation cross sec-

TABLE V. Absorption Oscillator Strengths for Be^+.

Transition	Present	NIST[a]	% Diff.
$2s$-$2p$	5.04[−1][b]	5.07[−1]	0.6
$2s$-$3p$	7.98[−2]	8.02[−2]	0.5
$2p$-$3s$	6.55[−2]	6.65[−2]	1.5
$2p$-$3d$	6.40[−1]	6.52[−1]	1.9
$3s$-$3p$	8.32[−1]	8.43[−1]	1.3
$3s$-$4p$	6.58[−2]	6.90[−2]	4.7
$3p$-$3d$	8.12[−2]	8.06[−2]	0.7
$3p$-$4s$	1.37[−1]	1.35[−1]	1.5
$3p$-$4d$	5.19[−1]	5.18[−1]	0.2
$3d$-$4f$	1.02	1.01	1.0

[a]See Ref. [26].
[b]$a[b]$ denotes $a\times10^b$.

tions from the $2s^2\,{}^1S$ ground term of beryllium to the $2s2p\,{}^3P$, $2s2p\,{}^1P$, and $2p^2\,{}^1D$ excited terms. For excitation to the $2s2p\,{}^3P$ term, we see, by comparing the curve from the 29-term *R*-matrix calculations with that from the RMPS calculation, that the effects of coupling to the target continuum are quite small for this spin-forbidden transition. However, for the dipole-allowed excitation to the $2s2p\,{}^1P$ term, the *R*-matrix result is about 20% higher than the RMPS result near the peak in the cross section. These effects are much more pronounced for the two-electron spin-allowed transition to the $2p^2\,{}^1D$ term, where the *R*-matrix cross section is more than 50% higher than the RMPS cross section at 20 eV.

As mentioned previously, electron-impact excitation data from both CCC calculations and earlier RMPS calculations have been reported in the literature. Cross sections from an RMPS calculation that used a much smaller pseudostate expansion than the one employed here were presented for excitations from the ground term to the $2s2p\,{}^{1,3}P$ terms by Bartschat *et al.* [7]; this was then extended to include all transitions from the ground term to the ten lowest excited terms by the same authors [8]. The results of CCC calculations for excitation from the ground term to the $2s2p\,{}^{1,3}P$

TABLE VI. Absorption oscillator strengths for Be^{2+}.

Transition	Present	NIST[a]	% Diff.
$1s^2\,{}^1S$-$1s2p\,{}^1P$	5.65[−1][b]	5.52[−1]	2.3
$1s^2\,{}^1S$-$1s3p\,{}^1P$	1.34[−1]	1.27[−1]	5.4
$1s2s\,{}^3S$-$1s2p\,{}^3P$	2.11[−1]	2.13[−1]	0.9
$1s2s\,{}^3S$-$1s3p\,{}^3P$	2.39[−1]	2.53[−1]	5.7
$1s2s\,{}^1S$-$1s2p\,{}^1P$	1.53[−1]	1.49[−1]	2.6
$1s2s\,{}^1S$-$1s3p\,{}^1P$	3.40[−1]	8.42[−1]	84.9
$1s2p\,{}^3P$-$1s3d\,{}^3D$	6.26[−1]	6.40[−1]	2.2
$1s2p\,{}^1P$-$1s3d\,{}^1D$	7.30[−1]	7.10[−1]	2.8
$1s3p\,{}^3P$-$1s3d\,{}^3D$	7.31[−2]	7.89[−2]	7.6
$1s3p\,{}^1P$-$1s3d\,{}^1D$	1.26[−2]	1.38[−2]	9.1

[a]See Ref. [26].
[b]$a[b]$ denotes $a\times10^b$.

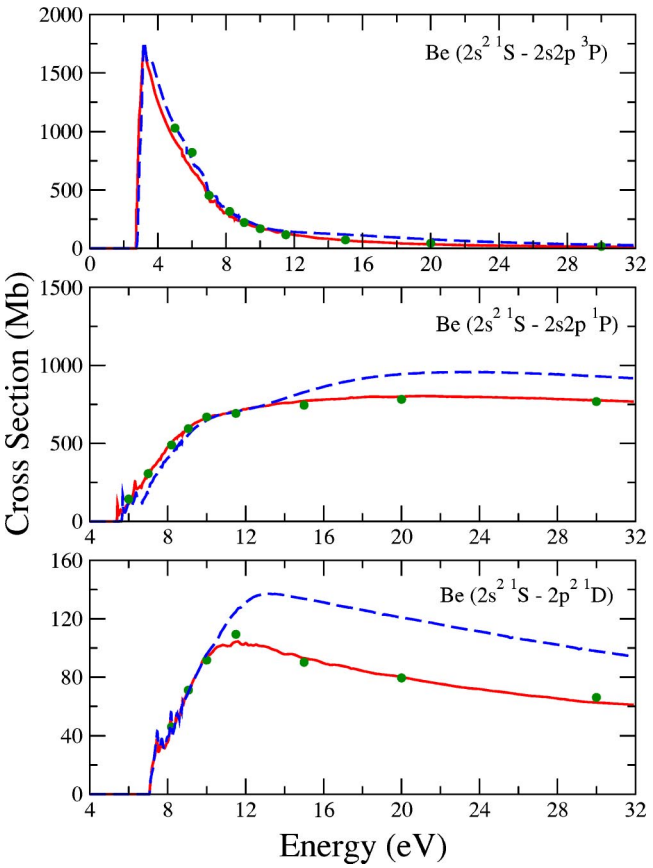

FIG. 1. Electron-impact excitation cross sections from the $2s^2\,{}^1S$ ground term of Be to the $2s2p\,{}^3P$, $2s2p\,{}^1P$, and $2p^2\,{}^1D$ excited terms. Dashed curves are from the present 29-term *R*-matrix calculation; solid curves are from the present 280-term RMPS calculation; solid circles are from CCC calculations as described in Fursa and Bray [9] and provided at the CCC database web site [11].

and $2p^2\,{}^2D$ terms were first reported by Fursa and Bray [9] and then extended to include all excitations from the ground state to the lowest 18 excited terms [10]. Bartschat *et al.* [8] and Fursa and Bray [9,10] also presented comparisons between the CCC and RMPS results. Finally, CCC data for excitation from the $2s^2\,{}^1S$ ground term and the $2s2p\,{}^{1,3}P$ excited terms are provided at the CCC database web site [11]. All the published results are presented in the form of graphs, some of which are on a logarithmic scale. Therefore, we have limited our comparisons in neutral beryllium to those tabulated at the aforementioned web site. These CCC data for excitation to the $2s2p\,{}^3P$, $2s2p\,{}^1P$, and $2p^2\,{}^1D$ terms are represented by the solid circles in Fig. 1, and are seen to be in excellent agreement with the present RMPS results.

In Fig. 2, we present results for excitation to both the ^3P and ^1P terms of the $2s3p$ and $2s4p$ configurations. For the spin-forbidden transitions to the ^3P terms, near the peak in the *R*-matrix cross sections, the *R*-matrix results are higher than the RMPS results by a factor of 2 for $n=3$ and a factor of 3 for $n=4$. The effects of coupling to the continuum are less pronounced for the two dipole-allowed transitions; however, the *R*-matrix cross sections are still over 40% higher

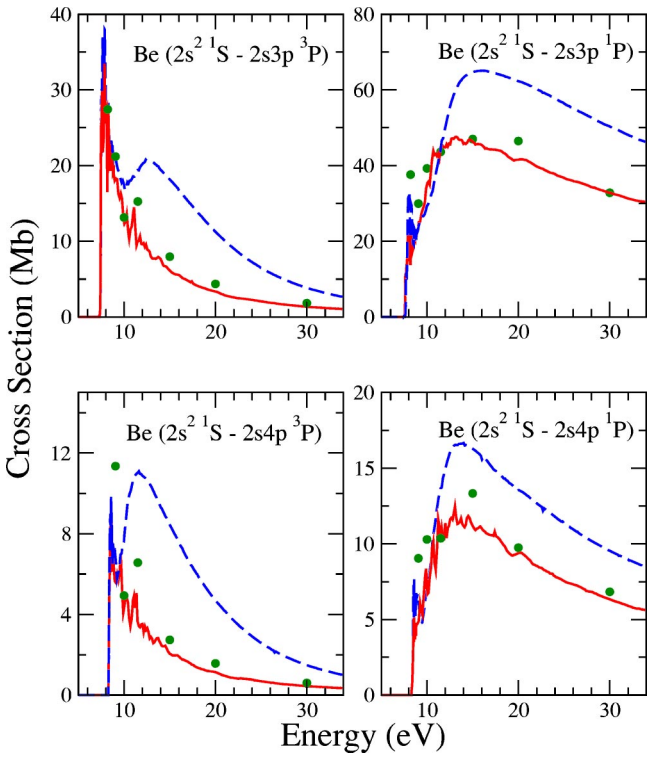

FIG. 2. Electron-impact excitation cross sections from the $2s^2\,{}^1S$ ground term of Be to the $2snp\,{}^3P$ and $2snp\,{}^1P$ excited terms for $n=3$ and 4. Dashed curves are from the present 29-term *R*-matrix calculation; solid curves are from the present 280-term RMPS calculation; solid circles are from CCC calculations as described in Fursa and Bray [10] and provided at the CCC database web site [11].

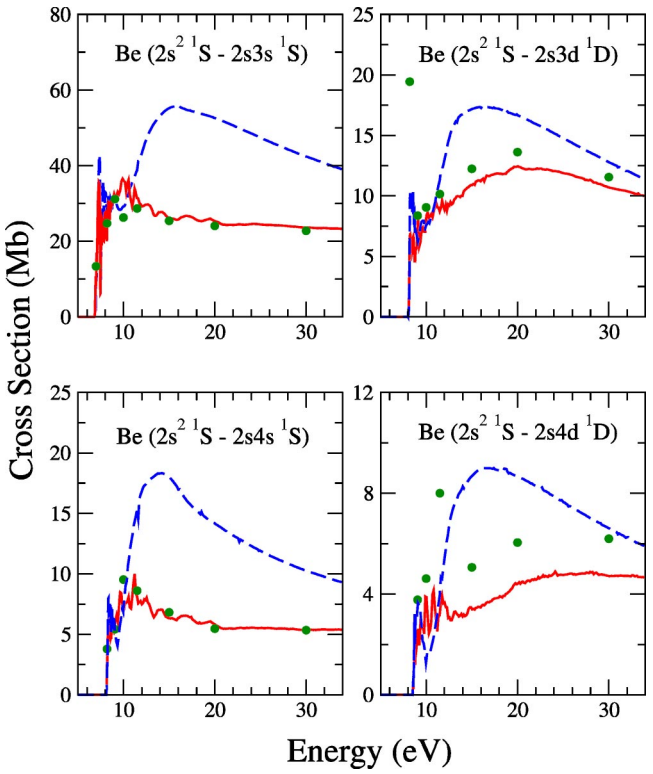

FIG. 3. Electron-impact excitation cross sections from the $2s^2\,{}^1S$ ground term of Be to the $2sns\,{}^1S$ and $2snd\,{}^1D$ excited terms. Dashed curves are from the present 29-term *R*-matrix calculation; solid curves are from the present 280-term RMPS calculation; solid circles are from CCC calculations as described in Fursa and Bray [10] and provided at the CCC database web site [11].

than those obtained from the RMPS calculations. We note that, at intermediate energies, the present results are in good agreement with the CCC cross sections; however, there does seem to be some scatter in the CCC data, especially at lower energies.

In Fig. 3, we show excitation cross sections from the $2s^2\,{}^1S$ ground term of Be to the $2sns\,{}^1S$ and $2snd\,{}^1D$ excited terms. Even though the effects of coupling to the continuum are larger for the spin-changing transitions than they are for the spin-allowed transitions shown here, we focus on the latter since they provide more meaningful comparisons with excitations in the Li-like and H-like Be ions. We see that the effects of coupling to the target continuum are larger for these spin-allowed nondipole transitions than they are for the dipole-allowed transitions considered above. For excitation to the $2sns\,{}^1S$ terms, the ratio of the 29-term *R*-matrix cross section to the RMPS cross section near the peak is about 2.0 for $n=3$ and has increased to 2.7 for $n=4$. In the case of excitation to the $2snd\,{}^1D$ terms, the ratio is 1.5 for $n=3$ and increases to 2.5 for $n=4$. We also note that, in the intermediate-energy range, our RMPS results are in excellent agreement with the CCC results for excitation to the $2sns\,{}^1S$ terms. However, the CCC cross sections are clearly higher than the RMPS values for excitation to the $2snd\,{}^1D$ terms; at 20 eV, the CCC values exceed the RMPS values by 11% for $n=3$ and by 38% for $n=4$. Furthermore, at lower energies, there is some large scatter in the CCC cross sections for these transitions.

The excitation cross sections for the $2s\rightarrow np$ transitions in Be^+ are shown in Fig. 4. As can be seen by comparing the RMPS and *R*-matrix cross sections, the effect of coupling to the target continuum for excitation to the $2p$ term is negligible and to the $3p$ term is small; however, this effect is much larger for excitation to the $4p$ term, where at the peak in the cross section, the *R*-matrix value is about 60% higher than the RMPS value. Also shown in this figure are the results of our TDCC calculations and they are seen to be in excellent agreement with those from the present RMPS calculations. As mentioned previously, cross sections from both CCC and earlier RMPS calculations for this ion are available in the literature [14]. They are found to be in good agreement with each other for excitation to the $2p$ and $3p$ terms; however, there are some noticeable differences between the two for excitation to the $4p$ term at low energies [14]. In Fig. 4, we show only the CCC results; they are seen to be in excellent agreement with the present RMPS and TDCC results for all three transitions.

The $2s\rightarrow ns$ and the $2s\rightarrow nd$ excitations for this ion are shown in Fig. 5. For these transitions, the effects of continuum coupling for excitation to the $n=3$ terms are much larger than they are for the corresponding dipole transitions. Moreover, at the peak in the cross sections, the ratio of the *R* matrix to RMPS values is about 1.8 for excitation to $4s$ and

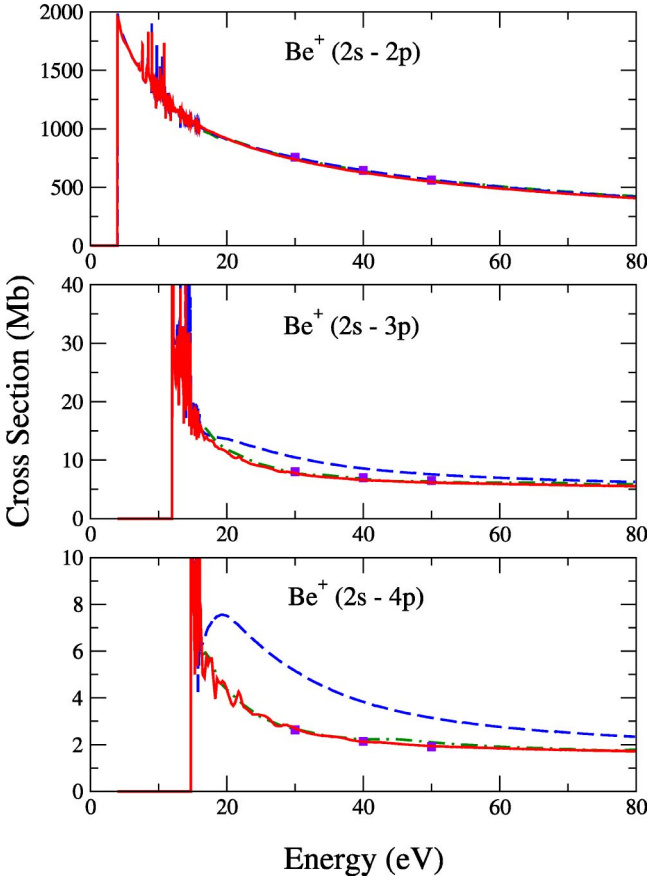

FIG. 4. Electron-impact excitation cross sections from the $2s$ ground term of Be^+ to the np excited terms. Dashed curves are from the present 14-term R-matrix calculation; solid curves are from the present 49-term RMPS calculation; solid squares are from the present TDCC calculation; dot-dashed curves from the CCC calculation by Bartschat and Bray [14].

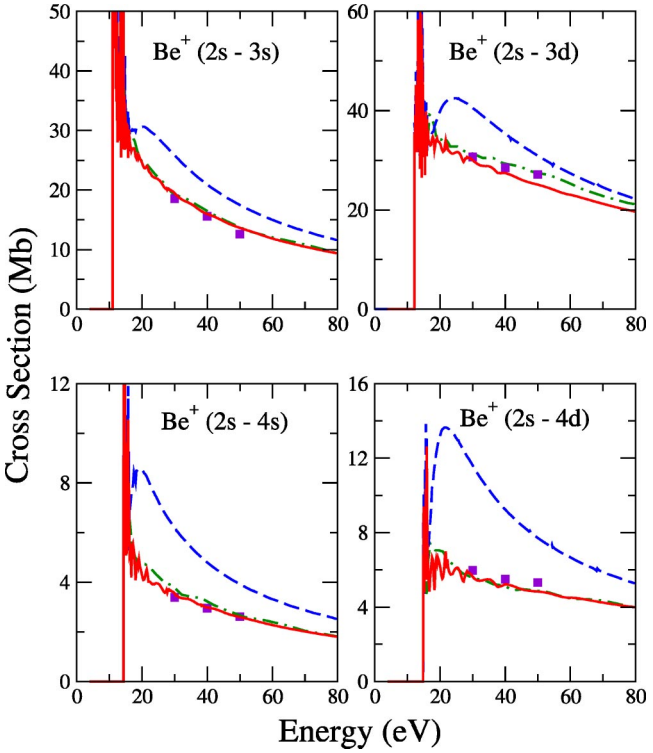

FIG. 5. Electron-impact excitation cross sections from the $2s$ ground term of Be^+ to the ns and nd excited terms. Dashed curves are from the present 14-term R-matrix calculation; solid curves are from the present 49-term RMPS calculation; solid squares are from the present TDCC calculation; dot-dashed curves from the CCC calculation by Bartschat and Bray [14].

about 2.3 for excitation to $4d$. Cross sections from the earlier CCC and RMPS calculations for excitation to the ns and nd terms appear to be in good agreement with each other [14], and here we only show the CCC results. The present RMPS, TDCC, and earlier CCC cross sections are in good agreement for the $2s \rightarrow ns$ excitations in the intermediate-energy range. For the $2s \rightarrow 3d$ transition, the TDCC and CCC results are somewhat larger than the RMPS cross section at the higher energies; for example, at 50 eV, the TDCC and CCC cross sections differ from the RMPS value by 8%. In the case of the $2s \rightarrow 4d$ excitation, the RMPS and CCC results are in excellent agreement at higher energies, but the TDCC results are from 5% to 10% higher. Nevertheless, the results from all of these nonperturbative calculations confirm the large effects of continuum coupling in this ion.

As mentioned earlier, we are not aware of any prior close-coupling calculations for Be^{2+}. Furthermore, the TDCC code, which describes the dynamics of two electrons in the continuum, is not capable of calculating term-to-term excitation cross sections in a system with more than one valence electron; therefore, TDCC calculations in a heliumlike system will have to await the development of a time-dependent code that fully describes the behavior of three correlated electrons. Work on this is currently in progress. For these reasons, our cross-section comparisons for Be^{2+} are restricted to those between our 29-term R-matrix calculation and our 103-term RMPS calculation. Such a comparison for the dipole-allowed excitations $1s^2\,{}^1S \rightarrow 1snp\,{}^1P$ and $1s2s\,{}^3S \rightarrow 1snp\,{}^3P$ are shown in Fig. 6.

As can be seen, coupling to the target continuum is pronounced for the excitations from the ground term; for example at 200 eV, the R-matrix cross sections are about 20%, 40%, and 60% above the RMPS cross sections for excitation to the $n=2$, $n=3$, and $n=4$ terms, respectively. For the excitations from the metastable term, continuum-coupling effects are negligible for the transitions to the $n=2$ and $n=3$ terms, but at 60 eV, they have increased to just over 20% for transitions to the $n=4$ term. The ratios of the R matrix to RMPS cross sections are much larger for excitations from the ground term, since these particular transitions tend to be dominated by the lower partial waves, which are the ones most affected by coupling to the target continuum. Although continuum coupling has larger effects in a neutral species, a similar trend is also seen for these transitions in neutral helium [28].

In Fig. 7, we present the excitation cross sections from $1s2s\,{}^3S$ metastable term to the $1sns\,{}^3S$ and $1snd\,{}^3D$ terms in Be^{2+}. We focus on the spin-allowed transitions from the metastable state in this ion, since they provide more meaningful comparisons with the spin-allowed transitions from

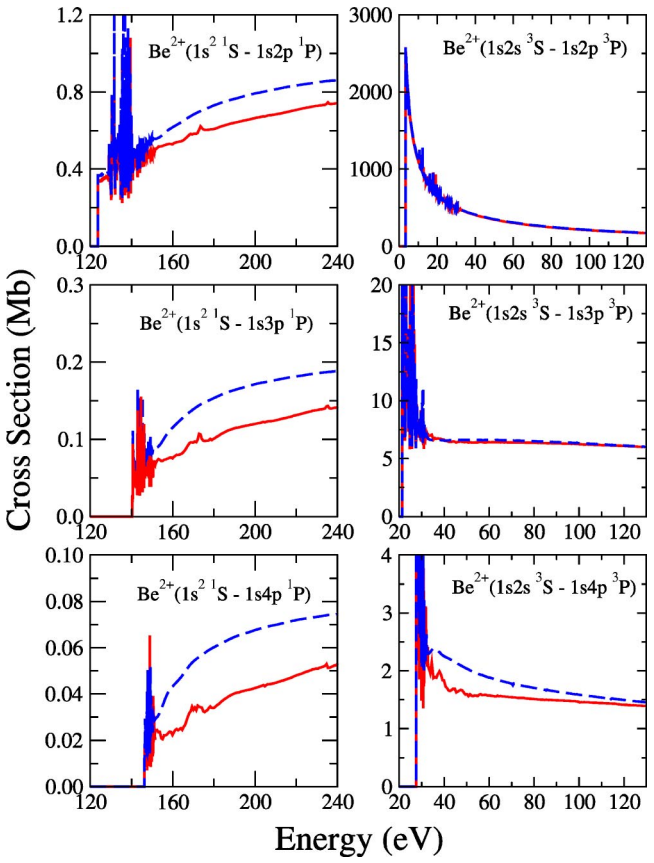

FIG. 6. Electron-impact excitation cross sections for Be^{2+} from the $1s^2\,{}^1S$ ground term to the $1snp\,{}^1P$ excited terms and from the $1s2s\,{}^3S$ metastable terms to the $1snp\,{}^3P$ excited terms. Dashed curves are from the present 29-term *R*-matrix calculation; solid curves are from the present 103-term RMPS calculation.

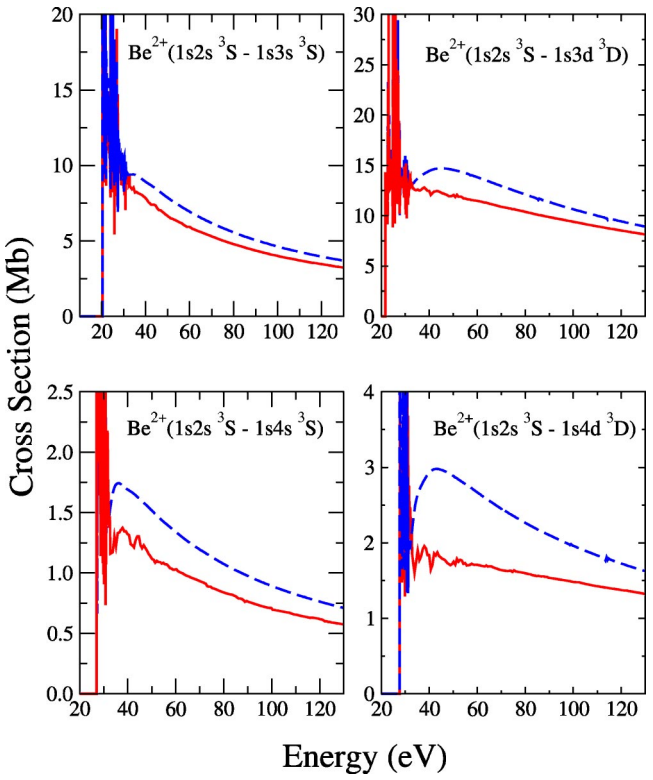

FIG. 7. Electron-impact excitation cross sections from the $1s2s\,{}^3S$ metastable term of Be^{2+} to the $1sns\,{}^3S$ and $1snd\,{}^3D$ excited terms. Dashed curves are from the present 29-term *R*-matrix calculation; solid curves are from the present 103-term RMPS calculation.

the ground state in Be as well as with the excitations from the ground state in Be^+. We see that, as in the cases of Be and Be^+, these dipole-forbidden transitions show larger effects due to coupling to the target continuum than the corresponding dipole-allowed transitions. Furthermore, these effects are still appreciable in this doubly ionized species, especially for excitation to the $n=4$ terms. Although not shown here, continuum coupling is even larger for excitations from the $1s^2\,{}^1S$ ground term to the $1sns\,{}^1S$ and $1snd\,{}^1D$ excited terms.

Finally, we consider electron-impact excitation of Be^{3+}. As mentioned earlier, RMPS results for this ion were recently reported by Ballance *et al.* [17] in a study of the hydrogen isoelectronic sequence. However, that paper only included comparisons with the DW calculations reported in the paper by Berrington and Clark [13]. Therefore, in order to complete the present study of continuum-coupling effects in the Be isonuclear sequence, we show our RMPS results in comparison with the results of a 15-term *R*-matrix calculation. We also show the results of our present TDCC calculation for excitation from the $2s$ metastable term.

In Fig. 8, we compare the cross sections for excitation to the $3p$ and $4p$ terms from the $1s$ ground term with those from the $2s$ metastable term. We have not included excitations to the $2p$ term in this figure since the continuum coupling effects for those transitions are quite small. As in the case of Be^{2+}, the effects of coupling to the target continuum in these dipole-allowed transitions are larger for transitions from the ground term than they are from the metastable term, again because of the importance of the low partial waves in the $1s\rightarrow np$ excitations. At 220 eV, the ratio of the *R* matrix to RMPS cross sections is 1.4 for the $1s\rightarrow 3p$ transition and 1.7 for the $1s\rightarrow\ 4p$ excitation. This ratio is small for the $2s\rightarrow 3p$ excitation, but at 60 eV, is 1.4 for the $2s\rightarrow 4p$ transition. The size of these continuum-coupling effects for dipole-allowed transitions in a triply ionized species is surprising.

Also shown in Fig. 8 are our TDCC cross sections for the $2s\rightarrow np$ excitations. They are somewhat higher than the RMPS results; for example, at 50 eV, the TDCC values differ from the RMPS cross sections by 12% and 6% for the $2s\rightarrow 3p$ and $2s\rightarrow 4p$ excitations, respectively. The fact that the TDCC cross section is slightly above the *R* matrix value for the $2s\rightarrow 3p$ excitation is not significant, since the effects of continuum coupling are clearly very small. However, the TDCC results do confirm the much larger effect of continuum coupling for the $2s\rightarrow 4p$ excitation.

In Fig. 9, we show the 15-term *R*-matrix, the 57-term RMPS, and the TDCC cross sections for excitation from the $2s$ metastable term to the ns and nd excited terms. Again, we focus on transitions from the metastable state in this ion to allow for comparisons with similar transitions in Be and

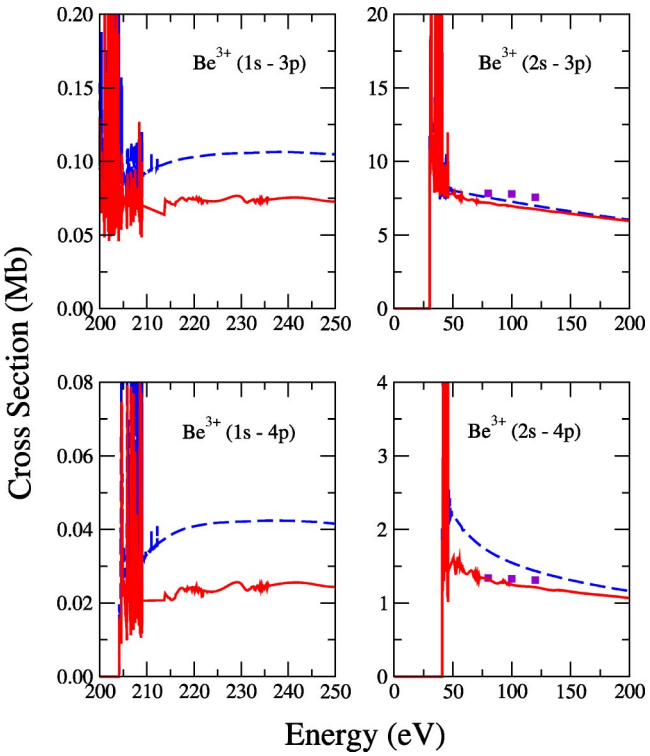

FIG. 8. Electron-impact excitation cross sections from the $1s$ ground term and the $2s$ metastable term of Be^{3+} to the np excited terms. Dashed curves are from the present 15-term R-matrix calculation; solid curves are from the present 57-term RMPS calculation; solid squares are from the present TDCC calculation.

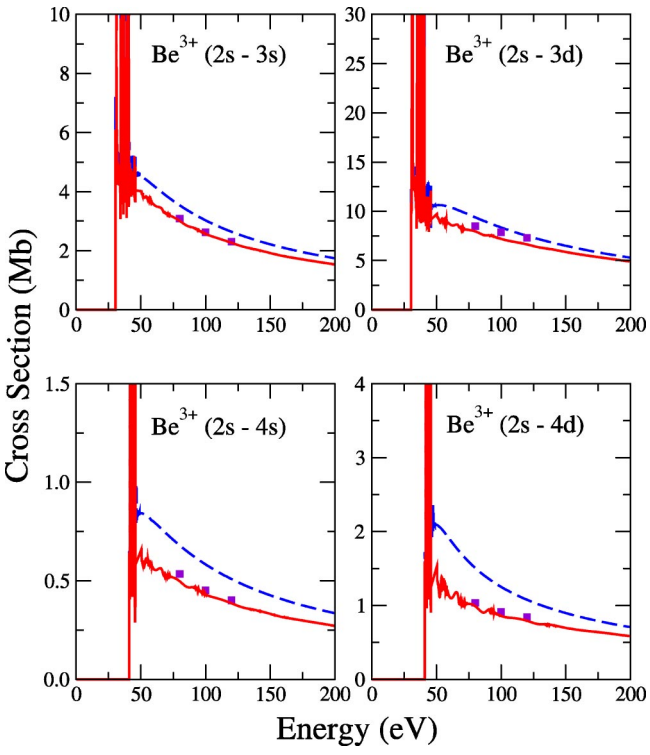

FIG. 9. Electron-impact excitation cross sections from the $2s$ metastable term of Be^{3+} to the ns and nd excited terms. Dashed curves are from the present 15-term R-matrix calculation; solid curves are from the present 57-term RMPS calculation; solid squares are from the present TDCC calculation.

its other ions. The RMPS and TDCC results are in good agreement for excitation to the ns terms. For this ion, there is also good agreement for the $2s \rightarrow 4d$ excitation; however, the TDCC cross sections are larger than the RMPS values by about 7% for the $2s \rightarrow 3d$ excitation. The effects of continuum coupling are still large, especially for excitation to the $n=4$ terms. For example, at 60 eV, the R-matrix cross sections are about 40% and 70% above the RMPS values for the $2s \rightarrow 4s$ and $2s \rightarrow 4d$ transitions, respectively; again this is surprising for a triply ionized species.

IV. CONCLUSIONS

We have completed an extensive set of R matrix with pseudostate calculations of electron-impact excitation for beryllium and all its ions. In addition, we have carried out time-dependent close-coupling calculations for excitation from the ground and metastable terms of Be^{+}, and the metastable term of Be^{3+}, and we have compared our RMPS cross sections with these as well as with some earlier convergent close-coupling calculations for Be and Be^{+}.

The TDCC, CCC, and RMPS methods are all capable of including the effects of coupling to the target continuum, which are important in atoms and low-charge-state ions in the intermediate-energy region. The TDCC and CCC methods have the advantage that, in general, they can be carried out to higher electron energies than the RMPS method, which is limited by the fact that the basis-set expansion used to represent the $(N+1)$-electron continuum becomes prohibitively large at high energies. However, to include an accurate description of the resonance contributions using either the CCC or TDCC methods would be prohibitively time consuming, since this would require separate close-coupling calculations at a very large number of energies. On the other hand, the RMPS method provides an efficient way to accurately describe the resonance contributions, which are important for the low-temperature modeling of fusion plasmas. Thus the present RMPS results represent the most complete set of excitation data for modeling applications of beryllium in the edge region of magnetically confined plasmas.

In addition to our RMPS calculations, we also performed standard R-matrix calculations that included the same target description, but did not include those pseudostates in the close-coupling expansion that were used to represent the high-Rydberg states and the target continuum. Since the target structure for these two calculations is identical, a comparison of the results of the RMPS and R-matrix calculations allowed us to determine the effects of coupling to the target continuum on electron-impact excitation cross sections. As one might expect, these effects are quite large in the neutral species, especially for excitations to the $n=4$ terms. However, they were also found to be significant in all stages of ionization, and in the case of the He-like and H-like species, are especially pronounced for excitation from the ground term.

Thus, if one wishes to generate accurate excitation cross

sections at intermediate energies in neutral and lower charge-state species, coupling of the bound states to the target continuum must be included. The size of the close-coupling expansion that is required in the RMPS calculations can present difficulties. In neutral beryllium, we included 280 terms in our close-coupling expansion, and even with the use of efficient parallel programs and massively parallel machines, such calculations become exceedingly time consuming. We have attempted to reduce these expansions, but have found that for certain types of transitions, this affects both the size of the pseudoresonances and the magnitude of the background cross sections. Of course, this presents more serious problems in complex species. For example, in an inert gas such as neon, LS coupling is no longer valid; therefore, one must perform a Breit-Pauli calculation to obtain level-to-level cross sections. The size of the RMPS close-coupling expansion nearly doubles and size of the $(N+1)$-electron matrices that must be considered increases by about a factor of 5. Whether such a calculation is even feasible with present massively parallel machines has not yet been determined. Clearly more work needs to be done on ways to include these continuum-coupling effects more efficiently.

ACKNOWLEDGMENTS

This work was supported in part by a U.S. DOE SciDAC grant (Grant No. DE-FG02-01ER54644), a U.S.-U.K. consortium through Auburn University, a DOE grant (Grant No. DE-FG02-99ER54367) to Rollins College, and a DOE grant (Grant No. DE-FG05-99ER5438) to Auburn University. The computational work was carried out at the National Energy Research Scientific Computing Center in Oakland, CA and at the Center for Computational Sciences in Oak Ridge, TN.

[1] J. Colgan, S.D. Loch, M.S. Pindzola, C.P. Ballance, and D.C. Griffin, Phys. Rev. A **68**, 032712 (2003).
[2] J. Colgan, M.S. Pindzola, A.D. Whiteford, and N.R. Badnell (unpublished).
[3] N.R. Badnell, J. Phys. B **30**, 1 (1997).
[4] P.O. Taylor, R.A. Phaneuf, and G.H. Dunn, Phys. Rev. A **22**, 435 (1980).
[5] W.C. Fon, K.A. Berrington, P.G. Burke, V.M. Burke, and A. Hibbert, J. Phys. B **25**, 507 (1992).
[6] R.E.H. Clark and J. Abdallah, Phys. Scr., T **T62**, 7 (1996).
[7] K. Bartschat, P.G. Burke, and M.P. Scott, J. Phys. B **29**, L769 (1996).
[8] K. Bartschat, P.G. Burke, and M.P. Scott, J. Phys. B **30**, 5915 (1997).
[9] D.V. Fursa and I. Bray, J. Phys. B **30**, L273 (1997).
[10] D.V. Fursa and I. Bray, J. Phys. B **30**, 5895 (1997).
[11] See http://atom.murdoch.edu.au/CCC-WWW/index.html
[12] J. Mitroy and D.W. Norcross, Phys. Rev. A **37**, 3755 (1988).
[13] K.A. Berrington and R.E.H. Clark, Nucl. Fusion Suppl. **3**, 87 (1992).
[14] K. Bartschat and I. Bray, J. Phys. B **30**, L109 (1997).
[15] A.K Pradhan, D.W. Norcross, and D.G. Hummer, Phys. Rev. A **23**, 619 (1981).
[16] N.R. Badnell, J. Phys. B **28**, 955 (1985).
[17] C.P. Ballance, N.R. Badnell, and E.S. Smyth, J. Phys. B **36**, 3707 (2003).
[18] D.M. Mitnik, D.C. Griffin, C.P. Ballance, and N.R. Badnell, J. Phys. B **36**, 717 (2003).
[19] T.W. Gorczyca, F. Robicheaux, M.S. Pindzola, D.C. Griffin, and N.R. Badnell, Phys. Rev. A **52**, 3877 (1995).
[20] A. Burgess, J. Phys. B **7**, L364 (1974).
[21] A. Burgess, D.G. Hummer, and J.A. Tully, Philos. Trans. R. Soc. London, Ser. A **266**, 225 (1970).
[22] D.C. Griffin, D.M. Mitnik, J. Colgan, and M.S. Pindzola, Phys. Rev. A **64**, 032718 (2001).
[23] M.K. Chen, J. Phys. B **31**, 4523 (1998).
[24] See http://www.vuse.vanderbilt. edu/~cff/mchf_collection
[25] G. Tachiev and C. Froese Fischer, J. Phys. B **32**, 5805 (1999).
[26] See http://physics.nist.gov/cgi-bin/AtData/lines_form
[27] See http://www-cfadc.phy.ornl.gov/data_and_codes
[28] C.P. Ballance, N.R. Badnell, D.C. Griffin, and H.P. Summers (unpublished).
[29] NIST Atomic Spectra Database: http://physics.nist.gov/cgi-bin/AtData/main_asd